

## The use of the empirical crack orientation tensor to characterize the damage anisotropy

Ludwig Schöttl, Wilfried V. Liebig, Kay A. Weidenmann, Kaan Inal, Peter Elsner

### Angaben zur Veröffentlichung / Publication details:

Schöttl, Ludwig, Wilfried V. Liebig, Kay A. Weidenmann, Kaan Inal, and Peter Elsner. 2021. "The use of the empirical crack orientation tensor to characterize the damage anisotropy." Composites Communications 25: 100613.  
<https://doi.org/10.1016/j.coco.2020.100613>.



# The use of the empirical crack orientation tensor to characterize the damage anisotropy

Ludwig Schöttl<sup>a,\*</sup>, Wilfried V. Liebig<sup>a,b</sup>, Kay A. Weidenmann<sup>b,c</sup>, Kaan Inal<sup>d</sup>, Peter Elsner<sup>a,b</sup>

<sup>a</sup> Karlsruhe Institute of Technology, Institute for Applied Materials, Engelbert-Arnold-Straße 4, 76131, Karlsruhe, Germany

<sup>b</sup> Fraunhofer Institute for Chemical Technology, Joseph-von-Fraunhofer-Straße 7, 76327, Pfinztal, Germany

<sup>c</sup> University of Augsburg, Institute of Materials Resource Management, Werner-von-Siemens-Straße 6, 86159, Augsburg, Germany

<sup>d</sup> University of Waterloo, Department of Mechanical and Mechatronics Engineering, 295 Philip Street, N2L 3G1, Waterloo, Canada

## ARTICLE INFO

### Keywords:

Fiber-reinforced polymer  
Micro-computed tomography  
In-situ testing  
Damage characterization

## ABSTRACT

In practice, a dominant failure mode of brittle materials, such as fiber-reinforced thermosets is the initiation and propagation of cracks under cyclic loading. In general, the damage in composites with irregular microstructure do not occur in regular patterns. There are several state-of-the-art continuum mechanical models which take the anisotropic damage for predicting the material behavior into account. Since damage generally occurs in an anisotropic way, methods that experimentally characterize the damage anisotropy are needed.

Micro-Computed Tomography systems ( $\mu$ CT) acquire volumetric images in a non-destructive way. By combining  $\mu$ CT scanning and mechanical in-situ testing, detailed microstructure data of specimens under load are generated. Based on image processing methods, the damage propagation from crack initiation to fracture is analyzed. In practice, cyclic load is a common load case for many components. Consequently, fatigue and cycle load tests are essential for a comprehensive material characterization.

In this contribution interrupted in-situ  $\mu$ CT tests with cyclic tensile load are performed on Sheet Molding Compounds (SMC), a discontinuous glass fiber-reinforced thermset composite. Image processing methods are introduced for the experimental determination of the anisotropic damage characteristic based on volumetric images. The methods enable analyzing the spatial crack orientation distribution. In order to quantify the damage anisotropy, empirical formulations of the crack density distribution and second-order crack orientation tensor are applied. The presented work in this contribution extends the results of preliminary experimental damage investigations. In addition to previous studies, the damage anisotropy is quantified and analyzed.

## 1. Introduction

The deformation behavior and mechanical properties of brittle materials, including fiber-reinforced thermosets are of great interest in many applications. In most cases, the inelastic deformation and fracture of brittle materials derive from crack initiation and propagation on the microstructural level. In general, as a consequence of anisotropic mechanical properties and multi-axial load, crack initiation and propagation occurs in an anisotropic way. In return cracks affect the material behavior on the macro-scale. In case the crack orientations are non-uniformly distributed, the resulting macroscopic mechanical material behavior is generally also anisotropic.

The authors Lubarda et al. [1] and Kachanov [2–4] proposed a method for mathematically describing the spatial crack distribution.

Based on the work of Onat et al. [5] the crack distribution is expanded in a Fourier-type tensor series. Furthermore, the authors Lubarda et al. [1] applied the crack density distribution and tensor approach to the experimental data by Hallbauer et al. [6] on micro-cracking studies in quartzite. The basic crack orientation tensor approach enables to take anisotropic damage into account for modern continuum mechanical models. Material models for the prediction of mechanical properties under the consideration of cracks were presented by several authors for brittle materials in general [3,4,7,8] and for fiber-reinforced composites in particular [9–16].

There are many different methods to experimentally investigate cracked solids [17,18]. Micro-Computed Tomography ( $\mu$ CT) is the technique of choice to acquire volumetric data of specimens in a non-destructive way. Through combining mechanical testing and in-situ

\* Corresponding author.

E-mail address: [ludwig.schoettl@kit.edu](mailto:ludwig.schoettl@kit.edu) (L. Schöttl).

$\mu$ CT scanning, volumetric images of damaged specimens under load are generated directly. Adapted to different material systems, load conditions and scanning techniques, there is a wide range of different in-situ  $\mu$ CT setups [19]. The authors Hufenbach et al. [20] proposed an in-situ  $\mu$ CT setup to apply superimposed tensile and torsion load. In addition the capability of ex-situ and in-situ  $\mu$ CT experiments are discussed in the work of Böhm et al. [21]. Different damage mechanism of fiber-reinforced polymers were characterized by means of in-situ and ex-situ tests [22,23]. In particular different damage mechanisms of fiber-reinforced polymers under fatigue load were studied by several authors [24–28].

The authors Schöttl et al. [29] analyzed the damage propagation of Sheet Molding Compounds (SMC) by means of interrupted in-situ  $\mu$ CT testing. The damage was applied in a controlled manner by cyclical tensile loading, which was gradually increased in each load step. By means of image processing the authors Schöttl et al. characterized the damage propagation based on the acquired volumetric images. Furthermore, the damage state is quantified by using the introduced crack volume fraction. Although the crack volume fraction quantifies the total damage state, it does not indicate the spatial damage anisotropy.

The results and methods introduced in this contribution extend the preliminary damage investigations of Schöttl et al. [29] by an anisotropic damage characterization. In this contribution the damage propagation of SMC is studied by means of in-situ  $\mu$ CT testing. An image processing method to analyze the spatial crack orientations based on volumetric images are presented. To characterize the damage anisotropy, an empirical formulation of the crack orientation tensor by Lubarda et al. [1] and Kachanov [2–4] is applied.

## 2. Method

### 2.1. Empirical crack orientation tensor

In general, as a consequence of anisotropic mechanical properties and multi-axial load, damage occurs in an anisotropic manner. In order to mathematically describe the spatial damage status, the authors Lubarda et al. [1] make use of the crack density distribution  $\rho(\mathbf{g})$ . It is assumed that cracks are planar and the crack orientation is represented by its normal vector  $\mathbf{g}$ , as shown in Fig. 1.

The total crack density  $\rho_0$  is obtained by integrating the crack density  $\rho$  over all spatial directions in Equation (1).

$$\rho_0 = \oint \rho(\mathbf{g}) d\mathbf{g} \quad (1)$$

By introducing the second-order crack density tensor  $\mathbf{P}$ , the crack density distribution  $\rho(\mathbf{g})$  can be approximated by

$$\rho(\mathbf{g}) = \mathbf{P} \cdot (\mathbf{g} \otimes \mathbf{g}), \quad (2)$$

Defining the symmetric second-order crack orientation tensor  $\mathbf{D}$

$$\mathbf{D} = \oint \rho(\mathbf{g}) \mathbf{g} \otimes \mathbf{g} d\mathbf{g}, \quad (3)$$

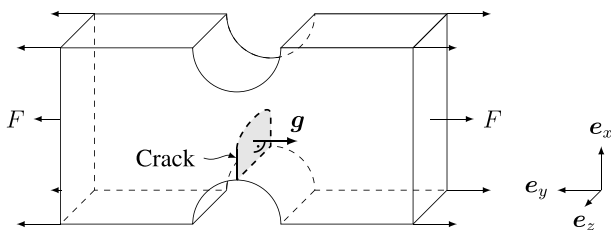


Fig. 1. General description of the orientation of planar cracks based on the normal vector  $\mathbf{g}$ .

according to Lubarda et al. [1] the second-order crack density tensor is substituted by

$$\mathbf{P} = \frac{15}{8\pi} \left( \mathbf{D} - \frac{\rho_0}{5} \mathbf{I} \right), \quad (4)$$

where  $\mathbf{I}$  is the second-order identity tensor. This means that the entire anisotropic fraction of  $\mathbf{P}$  is represented by  $\mathbf{D}$ . To experimentally analyze the anisotropic damage characteristics an empirical formulation for  $\rho_0$  and  $\mathbf{D}$  is introduced in this publication.

It is assumed that cracks are step-wise planar and the local orientation is indicated by unit vectors  $\mathbf{g}_i$  that are normal to the crack surface. Fig. 2 schematically illustrates the crack normal vectors  $\mathbf{g}_i$ . By adapting the work of Ken-Ichi [30] and Advani et al. [31] on fiber orientation tensors, the crack density distribution  $\rho(\mathbf{g})$  is expressed empirically based on  $N$  experimental crack normal vectors  $\mathbf{g}_i$  by

$$\rho(\mathbf{g}) = \frac{1}{N} \sum_{i=1}^N \delta(\|\mathbf{g} - \mathbf{g}_i\|), \quad (5)$$

where  $\delta(\cdot)$  is the Dirac delta function. Subsequently, the second-order crack orientation tensor  $\mathbf{D}$  in Equation (3) is empirically obtained by the sum

$$\mathbf{D} = \frac{1}{N} \sum_{i=1}^N \mathbf{g}_i \otimes \mathbf{g}_i. \quad (6)$$

Since the crack normal vectors are normed ( $\|\mathbf{g}_i\| = 1$ ), the first invariant of the empirical second-order crack orientation tensor becomes

$$\text{tr}(\mathbf{D}) = 1 = \rho_0. \quad (7)$$

As a consequence, the total crack density  $\rho_0$  is normalized to 1.

### 2.2. Crack normal vectors

In this contribution the crack propagation is investigated by means of in-situ  $\mu$ CT scanning. As a result, gray-value volumetric images of different damage stages are acquired. Cracks are voxel-wise segmented by applying image processing methods. The work in this contribution is based on the crack segmentation results of Schöttl et al. [29], in which cracks are segmented by means of the seed-region-growth approach by Adams et al. [32]. A representative cross section with a segmented crack is illustrated in Fig. 3 a). To overcome voxel-related discretization effects and to close the crack surface, slight Gaussian smoothing is applied in Fig. 3 b). Subsequently, the crack normal vectors are determined by using the spatial image gradient operator. The gradient operator applies the spatial Sobel-filter with a kernel size of 3-by-3-by-3 [33,34]. The crack normal vectors are determined subsequently, by assembling and normalizing the gradient images of all three spatial directions  $\mathbf{g} = (g_x, g_y, g_z)^T$ . For calculating the empirical crack orientation tensor  $\mathbf{D}$  only

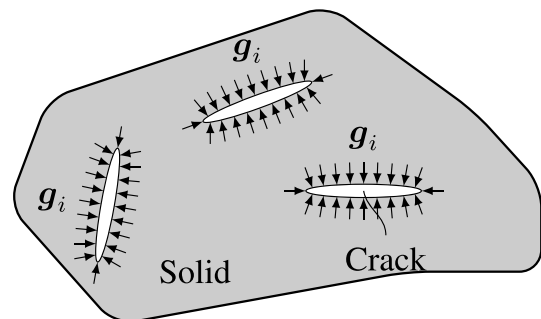
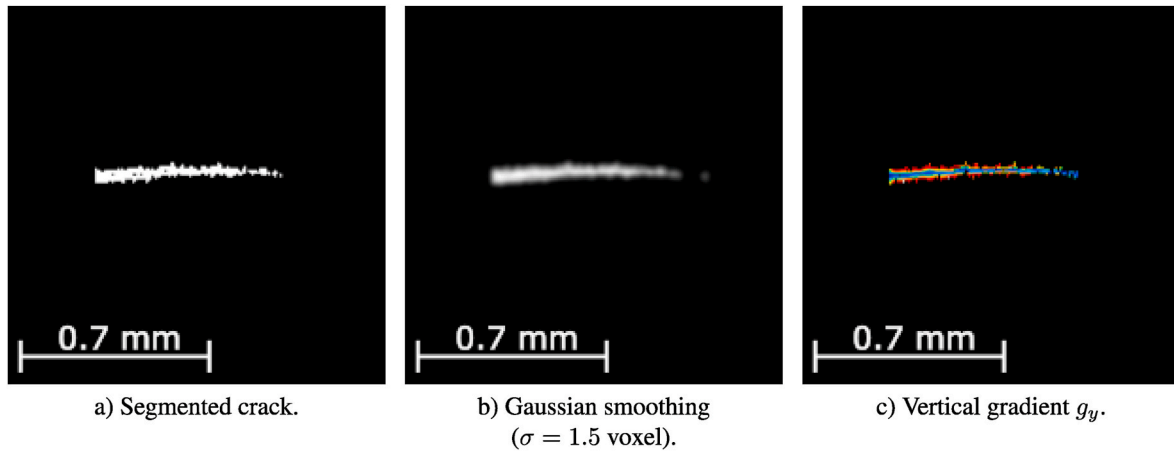


Fig. 2. Quantifying the crack orientation based on experimental data. Introducing the unit vectors  $\mathbf{g}_i$  normal to the crack surfaces.



**Fig. 3.** Image processing method to determine the crack normal vectors  $g_i$ . In a) a representative cross section with a voxel-wise segmented crack, in b) the Gaussian smoothing result ( $\sigma = 1.5$  voxel) and in c) the gradient in vertical direction (background in black, the crack in white and voxel size of  $6.8 \mu\text{m}$ ) is shown.

the crack normal vectors  $g$  at initial segmented voxels are used. Fig. 3 c) shows the vertical gradient  $g_y$  for those initial segmented voxels.

### 3. Experimental

#### 3.1. In-situ $\mu\text{CT}$ setup

The applied in-situ  $\mu\text{CT}$  setup is shown in Fig. 4 a) to Fig. 4 c) [35,36]. Due to the lean load frame the in-situ  $\mu\text{CT}$  setup can be placed close to the focus point and high-resolution images are acquired. The load frame is made of carbon fiber-reinforced polymers so that projections with low-noise are generated. The in-situ  $\mu\text{CT}$  setup and test procedure are introduced and discussed in the contribution of Schöttl et al. [29]. The selected test parameters including the mean displacement  $u_m$ , the displacement amplitude  $\Delta u$ , the number of cycles  $N_c$  and the frequency  $f$  are listed in Table 1. Fig. 5 shows the displacement  $u$  and nominal stress  $\sigma_N$  curve during the in-situ  $\mu\text{CT}$  test. The cyclic load is applied displacement controlled and the mean displacement is increased by 0.3 mm in each load step. In total four load steps are carried out until the specimen fractured. The test details and results of one examined SMC sample are presented and discussed in this contribution.

#### 3.2. Image acquisition

The in-situ  $\mu\text{CT}$  tensile test setup is installed inside a laboratory  $\mu\text{CT}$ -system of YXLON with a reflection tube by Comet. Resolution of the PerkinElmer flat panel Y.XRD1620 detector is  $2048 \text{ pixels} \times 2048 \text{ pixels}$

**Table 1**

Selected load step parameters of the performed in-situ  $\mu\text{CT}$  test. The mean displacement  $u_m$  is step-wise increased in each load step (data by Schöttl et al. [29]).

Parameters	Initial	Load step				Fracture	
		1	2	3	4		
$u_m$	mm	–	1.1	1.4	1.7	2.0	–
$\Delta u$	mm	–	$\pm 0.1$	$\pm 0.1$	$\pm 0.1$	$\pm 0.1$	–
$N_c$	–	–	100	100	100	100	–
$f$	Hz	–	0.067	0.067	0.067	0.067	–
$\sigma_{N,max}$	MPa	19.4	160.5	192.7	209.8	227.9	231.7

with a pixel pitch of  $200 \mu\text{m}$ . The  $\mu\text{CT}$  scans presented in this contribution are acquired with an acceleration voltage, current, exposure time and frame binning of 150 kV, 0.2 mA, 500 ms and 2, respectively. The  $\mu\text{CT}$  scanning process takes 80 min per load step to complete. The resulting volumetric images are reconstructed through 1950 projections over  $360^\circ$  and the VG STUDIO MAX 3.3 software by Volume Graphics. The isotropic voxel edge length of the reconstructed volumetric images is  $6.8 \mu\text{m}$ .

#### 3.3. Material

The introduced crack characterization methods and in-situ  $\mu\text{CT}$  test are applied to SMC. The examined SMC specimen consists of an

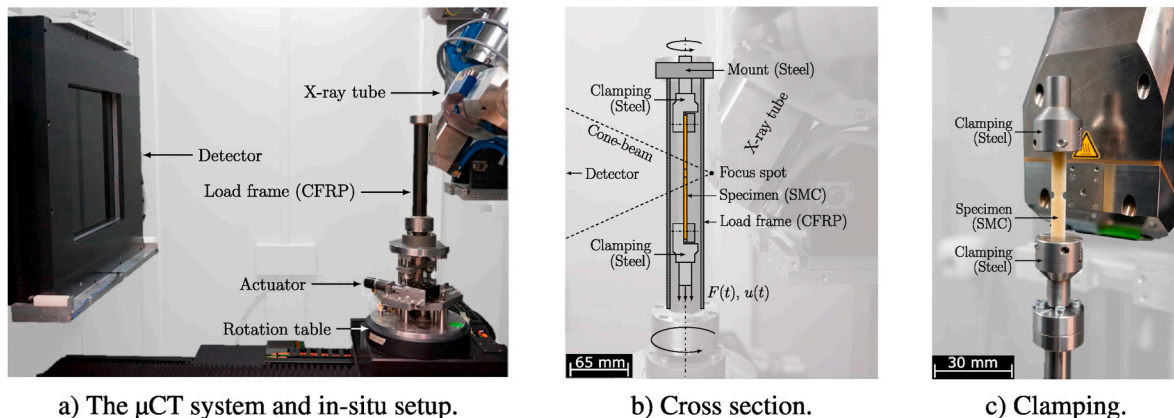


**Fig. 4.** Illustration of the  $\mu\text{CT}$  system and the in-situ testing setup. a) The detector, X-ray tube and the in-situ testing setup, b) the cross section of the in-situ setup and c) inner part of the in-situ setup including the SMC specimen and clamping (figures by Schöttl et al. [29]).

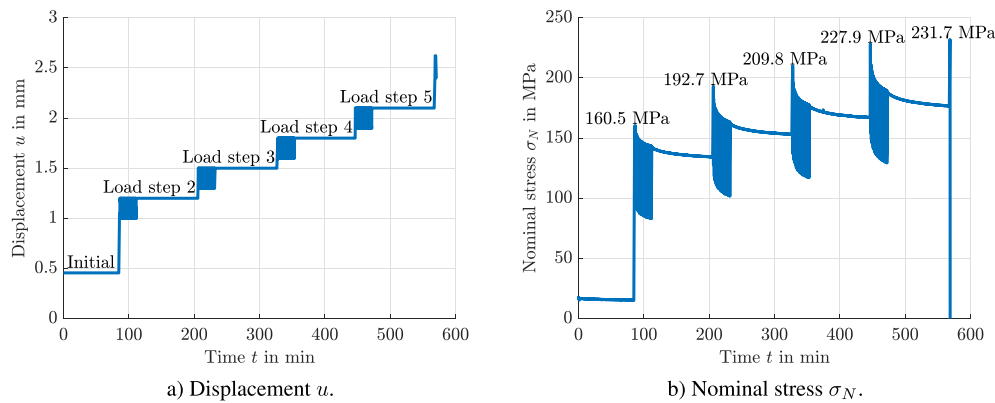


Fig. 5. Displacement controlled in-situ  $\mu$ CT test with cyclic tensile load. Initial and after each load step the specimen is screened by means of  $\mu$ CT scanning. In a) the displacement  $u$  and b) the nominal stress  $\sigma_N$  during the in-situ  $\mu$ CT test are plotted (data by Schöttl et al. [29]).

Unsaturated Polyester Polyurethane Hybrid (UPPH) matrix system without fillers from Aliancys, which is reinforced by 25.4 mm long glass fibers (GF Multistar 272) from Johns Manville. The nominal batch fiber weight content of the composite is 41 wt.%.

For manufacturing of the semi-finished SMC a carrier foil is covered with a thin layer of UPPH resin. The glass fiber rovings are then cut into uniform length of 25.4 mm and drop randomly oriented onto the UPPH resin layer. Subsequently, the composite is covered by another UPPH layer and carrier foil. The composite then passes through several cantilever rollers, whereby the fibers are infiltrated by the UPPH resin. After maturation, the semi-finished SMC is formed into plates of 800 mm  $\times$  250 mm by press molding. The examined specimen geometry in Fig. 6 is extracted by water jet cutting.

#### 4. Results

The representative cross section in Fig. 7 a) shows the initial SMC microstructure. After each load step volumetric images of the damaged specimen are acquired by means of in-situ  $\mu$ CT scanning. The enlarged cross sections in Fig. 7 b) to e) show the damage propagation within the red box in Fig. 7 a).

During the first load step a crack is initiated. The crack continues to spread during the second and third load step. Several additional cracks occur in the fourth load step. After the last load step the specimen fractures immediately after increasing the load at a maximum nominal stress of 231.7 MPa. As a consequence the cross section in Fig. 7 e) shows the SMC microstructure close to the final fracture.

Cracks within the volumetric image series are segmented by means of the seed-region-growth segmentation [29,32]. The images in Fig. 8 a) to d) show the segmented cracks within the corresponding cross sections in Fig. 7 b) to e). The cracks are indicated by white and the background by black. In addition, Fig. 9 a) to d) visualize the segmented cracks three-dimensionally. The authors Schöttl et al. [29] analyzed the segmented cracks and determined the crack volume fraction  $\rho_{\text{Crack}}$  for all four load steps. The resulting data are plotted in Fig. 10.

In addition to the paper [29], the crack normal vectors  $g_i$  are

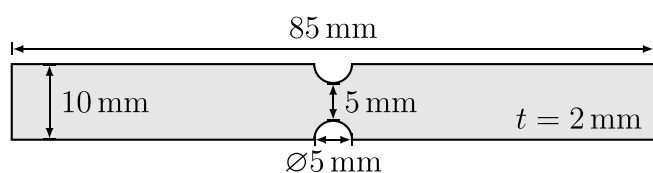


Fig. 6. The notched sample geometry used for the in-situ  $\mu$ CT test.  $\mu$ CT scanning provides high-resolution volumetric images of the region-of-interest around the notch.

determined and analyzed in this contribution. Fig. 11 a) to d) show the crack orientation histogram for all four load steps by means of polar plots. The crack orientation distribution of all four load steps is quantified statistically by using the empirical crack orientation tensors  $D$  in Fig. 13 a) to d). The results reveal, how the damage anisotropy develops during the in-situ  $\mu$ CT test. For comparison, the crack orientation histograms of all four load steps are plotted together in Fig. 12. Between first three load steps the principal crack orientation remains unchanged, but the crack orientation histogram becomes broader. In the fourth load step, additional cracks occur, as shown in Fig. 7 d) and the principal crack orientation changes approximately by 30°.

#### 5. Discussion

An in-situ  $\mu$ CT test series with cyclic tensile load and step-wise increasing mean displacement are carried out on SMC. The results in this contribution are based on the in-situ  $\mu$ CT test results presented in the work of Schöttl et al. [29]. As a result of stress concentration through the notch and the matrix rich region, cracks are formed at the notch center. The  $\mu$ CT cross sections in Figs. 7 and 8 together with the 3D-visualization in Fig. 9 show the crack initiation and propagation stages during the performed in-situ  $\mu$ CT test. In general, the minimum crack opening that can be segmented is limited by the voxel size. For  $\mu$ CT examination, the crack resolution is further affected by experimental aspects such as contrast and image noise. The authors analyzed the segmented cracks and concluded that cracks with a crack opening of two to three voxel are segmented reliably. The nominal stress response is shown in Fig. 5 b) and discussed in the paper of Schöttl et al. [29]. In total four load steps are performed. Immediately after the fourth load step the specimen fractured at a maximum nominal stress of 231.7 MPa. As a consequence, the volumetric image of the fourth load step shows the damaged microstructure close to the final fracture.

In the presented work, crack characterization methods are introduced and the damage anisotropy is studied. To quantify the crack orientations an empirical formulation of the second-order crack orientation tensor  $D$  is introduced in Equation (6). This enables to statistically summarized the crack orientations distribution based on experimental crack normal vectors  $g_i$ . Figs. 11, 12 and 13 show the crack orientation histograms and the corresponding second-order crack orientation tensors of all four load steps, respectively. The experimental data reveal how the spatial crack orientation changes due to the initiation of additional cracks and the propagation of the already existing ones.

The authors Lemaitre et al. [17,37] compared several methods for the experimental damage measurement. Furthermore, the size of representative volume elements for different materials are discussed. In case of polymers, the minimum length of representative volumes is 0.1 mm–1.0 mm. The width and thickness at the notch center of the

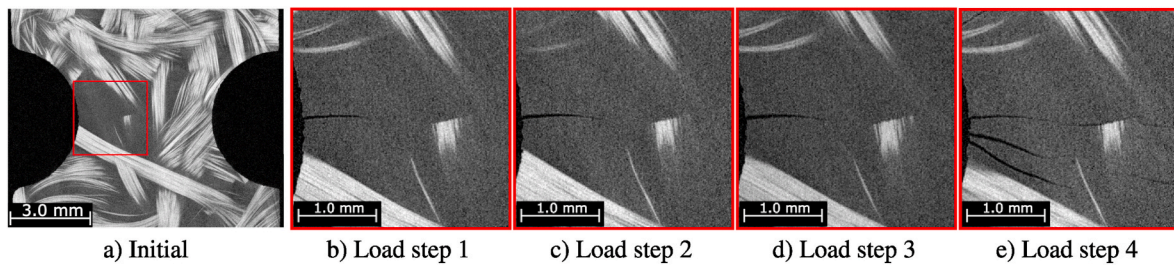


Fig. 7. The SMC damage propagation during the interrupted in-situ  $\mu$ CT test. In a) the initial and b) to e) the enlarged SMC microstructure after the respective load steps (figures by Schöttl et al. [29] and voxel size of  $6.8 \mu\text{m}$ ).

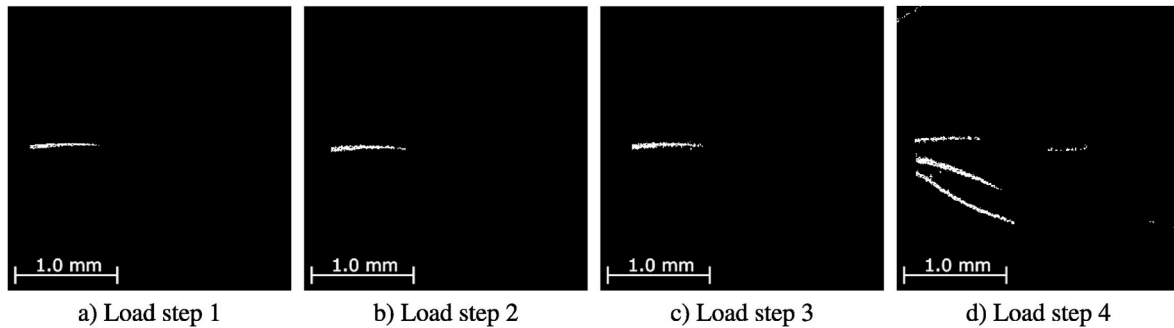


Fig. 8. The segmented cracks of the respective volumetric images corresponding to the cross sections in Fig. 7 b) to e). (image data by Schöttl et al. [29] and voxel size of  $6.8 \mu\text{m}$ ).

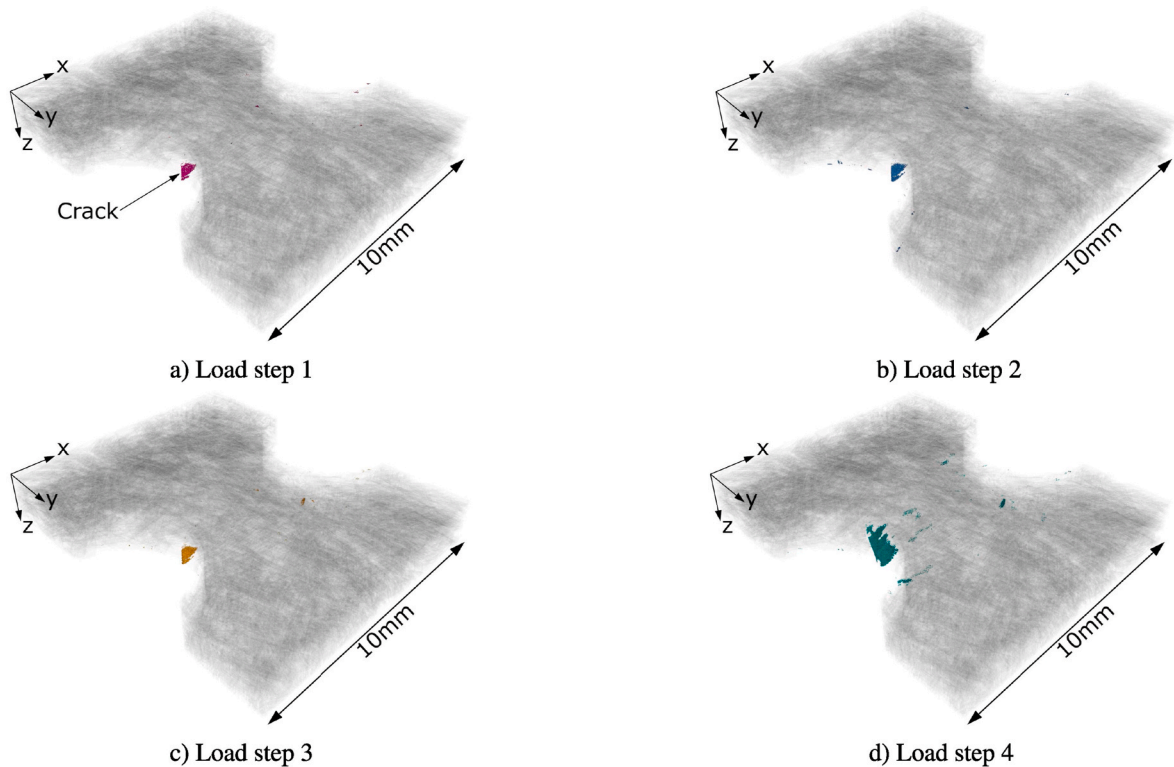
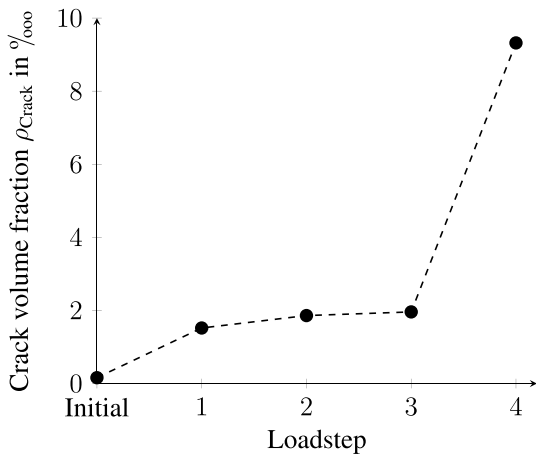


Fig. 9. The spatial crack propagation during the in-situ  $\mu$ CT test. 3D-visualization of the segmented cracks together with the SMC microstructure (transparent) for all four load steps.

examined specimen SMC are 5.0 mm and 2.0 mm, respectively. The authors Lubarda et al. [1] expanded the crack density distribution  $\rho$  in a tensor series to mathematically describe the crack orientations and to integrate them into continuum mechanic models for brittle materials.

The authors used the experimental data by Hallbauer et al. [6] on micro-cracking in quartzite. They determined the crack density distribution  $\rho$  by means of specimen cross sections and manual evaluation. Based on this data Lubarda et al. [1] calculated the second-order tensors



**Fig. 10.** Quantification of the total damage propagation during the in-situ  $\mu$ CT test. The crack volume fraction  $\rho_{Crack}$  initial and after all four load steps (data by Schöttl et al. [29]).

*D.* In contrast to this study,  $\mu$ CT scanning and image processing methods are used in this contribution to determine the spatial crack orientations. Subsequently, the second-order crack orientation tensor  $D$  is determined by applying the introduced empirical formulation in Equation (6). Due to the normalization the empirical crack orientation tensor  $D$  is independent of the number of crack norm vectors  $N$  and consequently, of the voxel size. As a consequence, the characterized damage anisotropy is generally valid and independent of the  $\mu$ CT scanning parameters. Furthermore, due to the normalization, the crack orientation tensor  $D$  can be specifically adapted to different problems such as the prediction of mechanical properties, heat conduction or permeability [2,4].

Although the material investigated in this contribution differs from that of Hallbauer et al. [6], the crack orientation histograms in Fig. 11 a) to d) and the results of Hallbauer et al. [6] reveal both typical brittle deformation phenomena, where the majority of crack normal vectors are oriented along to the tensile load direction. Assuming that the geometry of defects is known and simple, state-of-the-art continuum mechanic models and homogenization approaches can be applied to predict the effective material behavior [2,3,8,10]. In practice, the damage shape is generally complex and unknown. Especially for material systems with anisotropic material properties, such as fiber-reinforced composites. Consequently, the characterization and study of crack formation is essential for the investigation and prediction of the damage behavior.

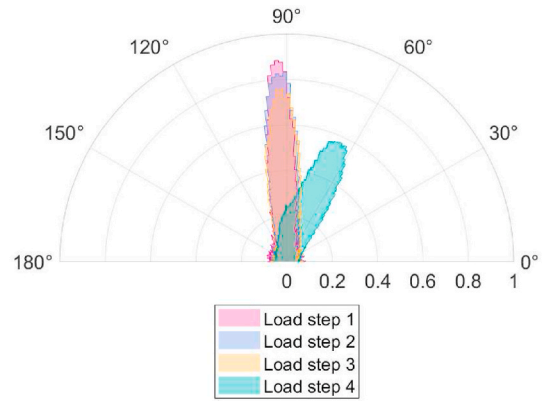
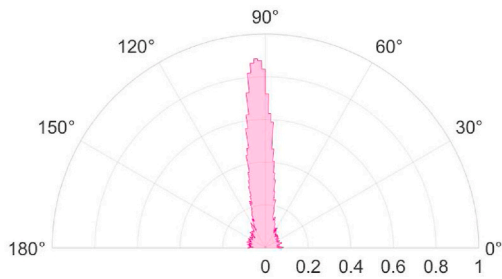
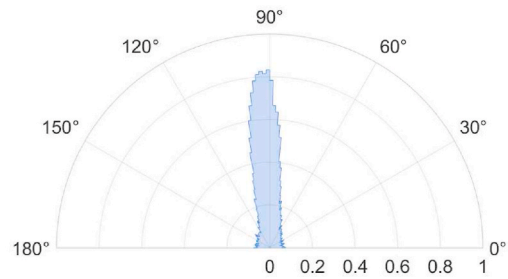


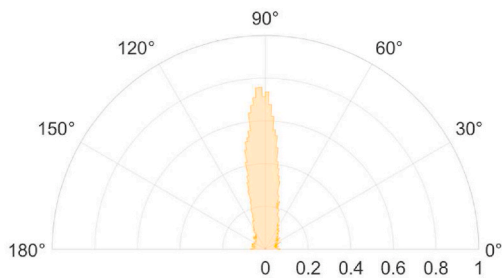
**Fig. 12.** The crack orientation histogram of all four load steps together. Between the third and fourth load step the principal crack orientation changes approximately by 30°. The axis  $e_x \hat{=} 0^\circ$  and  $e_y \hat{=} 90^\circ$ .



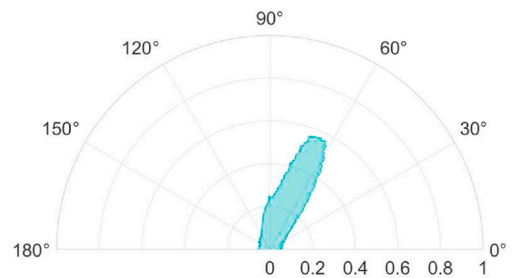
a) Load step 1



b) Load step 2



c) Load step 3



d) Load step 4

**Fig. 11.** The crack orientation histogram of all four respective load steps. In the first, second and third load step the principal crack orientation is aligned along the load direction. The axis  $e_x \hat{=} 0^\circ$  and  $e_y \hat{=} 90^\circ$ .

$$\begin{aligned}
 \mathbf{D} &= \begin{bmatrix} 0.10 & -0.05 & 0.00 \\ -0.05 & 0.81 & -0.01 \\ 0.00 & -0.01 & 0.09 \end{bmatrix}_{\{e_x, e_y, e_z\}} & \mathbf{D} &= \begin{bmatrix} 0.10 & -0.02 & 0.01 \\ -0.02 & 0.80 & -0.01 \\ 0.01 & -0.01 & 0.10 \end{bmatrix}_{\{e_x, e_y, e_z\}} \\
 \text{a) Load step 1} & & \text{b) Load step 2} & \\
 \\
 \mathbf{D} &= \begin{bmatrix} 0.10 & -0.02 & 0.00 \\ -0.02 & 0.82 & -0.01 \\ 0.00 & -0.01 & 0.08 \end{bmatrix}_{\{e_x, e_y, e_z\}} & \mathbf{D} &= \begin{bmatrix} 0.17 & 0.20 & 0.07 \\ 0.20 & 0.64 & 0.16 \\ 0.07 & 0.16 & 0.19 \end{bmatrix}_{\{e_x, e_y, e_z\}} \\
 \text{c) Load step 3} & & \text{d) Load step 4} &
 \end{aligned}$$

**Fig. 13.** The second-order crack orientation tensor  $\mathbf{D}$  quantifying the spatial crack distribution of all four respective load step. The crack orientation tensors show that in the first, second and third load step the crack orientation tensor fraction is aligned principally along the  $e_y$  axis.

The crack volume fraction  $\rho_{\text{Crack}}$  studied by Schöttl et al. [29], and illustrated in Fig. 10 characterizes the total damage state, but does not describe the spatial damage distribution. To overcome this issue, this contribution additionally introduces the empirical second-order crack orientation tensor  $\mathbf{D}$  to quantify the anisotropic characteristic of damage. The separation of scalar and tensorial damage description enables the adaption to various material systems and applications. To utilize the crack orientation tensor for predicting material properties (e.g. elastic deformation, fatigue and fluid filtration) appropriate scalar quantities have to be supplemented [2,4].

## 6. Conclusion

The results and methods presented in this contribution extend the work of Schöttl et al. [29]. The previous work focuses mostly on the experimental in-situ  $\mu$ CT test setup and the crack segmentation method. In this contribution an empirical formulation of the second-order crack orientation tensor is used to quantify the spatial damage distribution of Sheet Molding Compounds (SMC) in detail. The crack orientation tensor is determined based on experimental crack normal vectors. To analyze the spatial crack orientation in detail, interrupted in-situ  $\mu$ CT test with cyclic tensile load are carried out. As a result, high-resolution volumetric images of different damage propagation stages are acquired. The isotropic voxel size of the volumetric images is 6.8  $\mu\text{m}$ . Cracks with a minimum crack opening of two to three times the voxel size (13.6–20.4  $\mu\text{m}$ ) are segmented and analyzed. By applying the introduced image processing methods the local crack normal vectors are determined and subsequently the crack orientation tensor is calculated.

In addition to the study of Schöttl et al. [29], this contribution analyzes the damage anisotropy of brittle material from crack initiation to fracture of the specimen. The results show that close to the final fracture additional cracks emerge and consequently, the principal crack orientation is changed. The investigations in this contribution reveal that the empirical second-order crack orientation tensor and histogram are suitable to describe and quantify the damage anisotropy of brittle materials. Furthermore, the work demonstrates the applicability of in-situ  $\mu$ CT tests for the investigation of crack initiation and propagation on SMC. The methods and results in this contribution on anisotropic damage characterization complement the crack volume fraction data by Schöttl et al. [29]. Together, the crack volume fraction and the crack orientation tensor describe and quantify both, the total damage and the

spatial damage distribution.

## Authors contribution

Ludwig Schöttl developed, implemented and applied the methods presented in this paper. He also carried out the experimental tests and wrote the first draft of the paper. Wilfried V. Liebig, Kay A. Weidenmann and Peter Elsner supervised and coordinated the implementation and application by Ludwig Schöttl at the Karlsruhe Institute of Technology. Wilfried V. Liebig, Kay A. Weidenmann, Kaan Inal and Peter Elsner thoroughly revised the paper.

## CRedit authorship contribution statement

**Ludwig Schöttl:** Conceptualization, Methodology, Software, Formal analysis, Investigation, Writing – original draft, Visualization, Project administration. **Wilfried V. Liebig:** Conceptualization, Resources, Writing – review & editing, Supervision. **Kay A. Weidenmann:** Conceptualization, Resources, Writing – review & editing, Supervision, Funding acquisition. **Kaan Inal:** Conceptualization, Writing – review & editing, Supervision. **Peter Elsner:** Conceptualization, Resources, Writing – review & editing, Supervision, Funding acquisition.

## Declaration of competing interest

The authors declare that they have no known competing financial interests or personal relationships that could have appeared to influence the work reported in this paper.

## Acknowledgments

The research documented in this manuscript has been funded by the German Research Foundation (DFG) within the International Research Training Group “Integrated engineering of continuous-discontinuous long fiber reinforced polymer structures” (GRK 2078). The support by the German Research Foundation (DFG) is gratefully acknowledged.

Furthermore, the authors would also like to thank the Fraunhofer ICT for their support by providing the Sheet Molding Compound (SMC) plates, which were manufactured under the project leadership of Sergej Ilinzeer.

## Nomenclature

$\delta$	Dirac delta function
$\mathbf{D}$	Second-order crack orientation tensor
$\mathbf{g}$	Crack normal vector

$I$	Second-order identity tensor
$P$	Second-order crack density tensor
$\rho$	Crack density distribution
$\rho_0$	Total crack density
$\rho_{\text{Crack}}$	Crack volume fraction

## References

- [1] V.A. Lubarda, D. Krajcinovic, Damage tensors and the crack density distribution, *Int. J. Solid Struct.* 30 (20) (1993) 2859–2877.
- [2] M. Kachanov, Continuum model of medium with cracks, *J. Eng. Mech. Div.* 106 (5) (1980) 1039–1051.
- [3] M. Kachanov, Effective elastic properties of cracked solids: critical review of some basic concepts, *Appl. Mech. Rev.* 45 (8) (1992) 304–335.
- [4] M. Kachanov, Elastic solids with many cracks and related problems, in: *Advances in Applied Mechanics*, vol. 30, Elsevier, 1993, pp. 259–445.
- [5] E.T. Onat, F.A. Leckie, Representation of mechanical behavior in the presence of changing internal structure, *J. Appl. Mech.* 55 (1) (1988) 1–10.
- [6] D.K. Hallbauer, H. Wagner, N.G.W. Cook, Some observations concerning the microscopic and mechanical behaviour of quartzite specimens in stiff, triaxial compression tests, *Int. J. Rock Mech. Min. Sci. Geomech. Abstr.* 10 (6) (1973) 713–726.
- [7] C.M. Sayers, M. Kachanov, A simple technique for finding effective elastic constants of cracked solids for arbitrary crack orientation statistics, *Int. J. Solid Struct.* 27 (6) (1991) 671–680.
- [8] D. Halm, A. Dragon, A model of anisotropic damage by Mesocrack growth; unilateral effect, *Int. J. Damage Mech.* 5 (4) (1996) 384–402.
- [9] R. Talreja, Continuum modelling of damage in ceramic matrix composites, *Mech. Mater.* 12 (2) (1991) 165–180.
- [10] A. Matzenmiller, J. Lubliner, R.L. Taylor, A constitutive model for anisotropic damage in fiber-composites, *Mech. Mater.* 20 (2) (1995) 125–152.
- [11] F. Meraghni, C.J. Blakeman, M.L. Benzeggagh, Effect of interfacial decohesion on stiffness reduction in a random discontinuous-fibre composite containing matrix microcracks, *Compos. Sci. Technol.* 56 (5) (1996) 541–555.
- [12] F. Desrumaux, F. Meraghni, M.L. Benzeggagh, Micromechanical modelling coupled to a reliability approach for damage evolution prediction in composite materials, *Appl. Compos. Mater.* 7 (4) (2000) 231–250.
- [13] F. Desrumaux, F. Meraghni, M.L. Benzeggagh, Generalised Mori-Tanaka scheme to model anisotropic damage using numerical Eshelby tensor, *J. Compos. Mater.* 35 (7) (2001) 603–624.
- [14] W. Yang, Y. Pan, A.A. Pelegri, Multiscale modeling of matrix cracking coupled with interfacial debonding in random glass fiber composites based on volume elements, *J. Compos. Mater.* 47 (27) (2013) 3389–3399.
- [15] B. Raju, S.R. Hiremath, D.R. Mahapatra, A review of micromechanics based models for effective elastic properties of reinforced polymer matrix composites, *Compos. Struct.* 204 (2018) 607–619.
- [16] M. Schemmann, J. Görthofer, T. Seelig, A. Hrymak, T. Böhlke, Anisotropic meanfield modeling of debonding and matrix damage in SMC composites, *Compos. Sci. Technol.* 161 (2018) 143–158.
- [17] J. Lemaitre, J. Dufailly, Damage measurements, *Eng. Fract. Mech.* 28 (5) (1987) 643–661.
- [18] S. Gholizadeh, A review of non-destructive testing methods of composite materials, in: *XV Portuguese Conference on Fracture, PCF 2016*, vol. 1, 2016, pp. 50–57.
- [19] S.C. Garcea, Y. Wang, P.J. Withers, X-ray computed tomography of polymer composites, *Compos. Sci. Technol.* 156 (2018) 305–319.
- [20] W. Hufenbach, R. Böhm, M. Gude, M. Berthel, A. Hornig, S. Rucevskis, M. Andrich, A test device for damage characterisation of composites based on in situ computed tomography, *Compos. Sci. Technol.* 72 (12) (2012) 1361–1367.
- [21] R. Böhm, J. Stiller, T. Behnisch, M. Zschege, R. Protz, S. Radloff, M. Gude, W. Hufenbach, A quantitative comparison of the capabilities of in situ computed tomography and conventional computed tomography for damage analysis of composites, *Compos. Sci. Technol.* 110 (2015) 62–68.
- [22] F. Sket, A. Enfedaque, C. Alton, C. González, J.M. Molina-Aldareguia, J. Llorca, Automatic quantification of matrix cracking and fiber rotation by X-ray computed tomography in shear-deformed carbon fiber-reinforced laminates, *Compos. Sci. Technol.* 90 (2014) 129–138.
- [23] K. Wang, S. Pei, Y. Li, J. Li, D. Zeng, X. Su, X. Xiao, N. Chen, In-situ 3D fracture propagation of short carbon fiber reinforced polymer composites, *Compos. Sci. Technol.* 182 (2019) 107788.
- [24] P.J. Schilling, B.R. Karedla, A.K. Tatiparthi, M.A. Verges, P.D. Herrington, X-ray computed microtomography of internal damage in fiber reinforced polymer matrix composites, *Compos. Sci. Technol.* 65 (14) (2005) 2071–2078.
- [25] F. Cosmi, A. Bernasconi, Micro-CT investigation on fatigue damage evolution in short fibre reinforced polymers, *Compos. Sci. Technol.* 79 (2013) 70–76.
- [26] S.C. Garcea, M.N. Mavrogordato, A.E. Scott, I. Sinclair, S.M. Spearing, Fatigue micromechanism characterisation in carbon fibre reinforced polymers using synchrotron radiation computed tomography, *Compos. Sci. Technol.* 99 (2014) 23–30.
- [27] S.C. Garcea, I. Sinclair, S.M. Spearing, In situ synchrotron tomographic evaluation of the effect of toughening strategies on fatigue micromechanisms in carbon fibre reinforced polymers, *Compos. Sci. Technol.* 109 (2015) 32–39.
- [28] S.C. Garcea, I. Sinclair, S.M. Spearing, Fibre failure assessment in carbon fibre reinforced polymers under fatigue loading by synchrotron X-ray computed tomography, *Compos. Sci. Technol.* 133 (2016) 157–164.
- [29] L. Schöttl, P. Kolb, W.V. Liebig, K.A. Weidenmann, K. Inal, P. Elsner, Crack characterization of discontinuous fiber-reinforced composites by using micro-computed tomography: cyclic in-situ testing, crack segmentation and crack volume fraction, *Compos. Commun.* (2020) 100384.
- [30] K. Ken-Ichi, Distribution of directional data and fabric tensor, *Int. J. Eng. Sci.* 22 (2) (1984) 149–164.
- [31] S.G. Advani, C.L. Tucker, The use of tensors to describe and predict fiber orientation in short fiber composites, *J. Rheol.* 31 (8) (1987) 751–784.
- [32] R. Adams, L. Bischof, Seeded region growing, *IEEE Trans. Pattern Anal. Mach. Intell.* 16 (6) (1994) 641–647.
- [33] W.K. Pratt, *Introduction to Digital Image Processing*, Taylor & Francis Group, 2014.
- [34] A. Distanto, *Handbook of Image Processing and Computer Vision : Volume 2: from Image to Pattern*, 1 edition, Springer eBook Collection. Springer International Publishing, 2020.
- [35] A. Heni, Construction and Development of an In-situ Testing Setup for Computed Tomography, Bachelor's thesis, Karlsruhe Institute of Technology (KIT), 2012.
- [36] F. Pottmeyer, J. Bittner, P. Pinter, K.A. Weidenmann, In-situ CT damage analysis of metal inserts embedded in carbon fiber-reinforced plastics, *Exp. Mech.* 57 (9) (2017) 1411–1422.
- [37] J. Lemaitre, R. Desmorat, M. Sauzay, Anisotropic damage law of evolution, *Eur. J. Mech. Solid.* 19 (2) (2000) 187–208.